Spatial variations of P wave attenuation in the mantle beneath North America

Yong Keun Hwang,[1] Jeroen Ritsema,[1] and Saskia Goes[2]

Received 10 September 2008; revised 26 February 2009; accepted 17 April 2009; published 20 June 2009.

[1] We estimate the spatial variation of the seismic parameter t^* using teleseismic (epicentral distance = 30°–85°) P wave spectra of about 200 deep (focal depths > 200 km) earthquakes recorded by 378 broadband seismometers in the United States and Canada. Relative P wave spectral ratios up to 1 Hz for about 63,000 station pairs with high signal-to-noise ratio and impulsive P waveforms are inverted for t_P^* by least squares inversion. The continental-scale t_P^* pattern correlates to the age of geological terrains and the seismic, heat flow, gravity, and magnetic variations across North America. Predominantly low values of t_P^* are obtained in stable central North America (SNA), and high t_P^* values are obtained for stations in the tectonically active western part of the continent (TNA). This variation is similar to that observed previously in short-period amplitude anomalies, spectral ratio variations, and ScS reverberations. On average, we resolve a contrast in t_P^* between SNA and TNA of about 0.2 s. We resolve regional variations in t_P^*, which correlate with tectonics. Relatively low t_P^* is associated with currently active subduction below Alaska. Relatively high t_P^* is found in SNA below the Appalachians and the Gulf Coast. The consistency between t_P^* and tectonics suggests that the observed variations in t_P^* are, on the scale of around 200–500 km, predominantly due to intrinsic attenuation. The similar patterns in t_P^* and predicted values for a recent global attenuation model confirm this further. The compatibility with the t_P^* computed for attenuation estimated via a thermal interpretation of shear wave velocity anomalies illustrates that variations in seismic velocity are predominantly due to physical effects with a strong attenuation signature, most likely temperature or a combination of temperature and water content.

Citation: Hwang, Y. K., J. Ritsema, and S. Goes (2009), Spatial variations of P wave attenuation in the mantle beneath North America, *J. Geophys. Res.*, *114*, B06312, doi:10.1029/2008JB006091.

1. Introduction

[2] Models of seismic attenuation provide important constraints on the physical state of Earth's interior. Seismic wave attenuation and velocity dispersion [*Kanamori and Anderson*, 1977] are affected by temperature, by volatiles, and, depending on the dominant relaxation mechanism, by the presence of melt [*Sato et al.*, 1989; *Hammond and Humphreys*, 2000; *Faul and Jackson*, 2005]. Moreover, anelasticity provides one of the few available measures of rheology at lithosphere and mantle conditions, albeit on seismic timescales [*Karato and Spetzler*, 1990; *Jackson et al.*, 2002].

[3] Attenuation constraints are key in the interpretation of models of seismic velocity (i.e., seismic tomography) [*Sobolev et al.*, 1996; *Goes et al.*, 2000; *Goes and van der Lee*, 2002; *Lee*, 2003; *Godey et al.*, 2004; *Shapiro and Ritzwoller*, 2004; *Faul and Jackson*, 2005; *Deen et al.*, 2006; *Schutt and Lesher*, 2006]. These studies demonstrate that velocity variations in the uppermost mantle (<200–300 km) are primarily due to temperature variations because of the high temperature sensitivity to anelastic effects in this depth range [*Sato et al.*, 1989; *Karato*, 1993; *Goes et al.*, 2000; *Jackson et al.*, 2002; *Faul and Jackson*, 2005]. Variations in major element chemistry have a non-negligible contribution on velocity anomalies only in the coldest regions of the uppermost mantle, which can be resolved in combination with density-sensitive data [*Perry et al.*, 2003; *Godey et al.*, 2004; *Deen et al.*, 2006]. However, the interpretation of tomographic models is meaningful only when constraints on attenuation with comparable spatial resolution are available.

[4] On a global scale, tomographic images reveal seismic velocity structures that are only a few hundred kilometers in size [*Romanowicz*, 2008]. Global attenuation models are still designed to constrain long wavelength variations because the effects of intrinsic attenuation on wave amplitudes cannot be easily distinguished from the effects of wave scattering, focusing, and crustal amplification in a perfectly

[1]Department of Geological Sciences, University of Michigan, Ann Arbor, Michigan, USA.
[2]Department of Earth Science and Engineering, Imperial College London, London, UK.

0148-0227/09/2008JB006091$09.00

elastic but heterogeneous Earth. Global attenuation models based on surface waves [*Romanowicz*, 1995; *Billien et al.*, 2000; *Romanowicz and Gung*, 2002; *Selby and Woodhouse*, 2002; *Dalton and Ekström*, 2006], body waves [*Bhattacharyya et al.*, 1996; *Reid et al.*, 2001; *Warren and Shearer*, 2002; *Lawrence and Wysession*, 2006], and *Lg* coda [*Mitchell and Cong*, 1998] share similar large-scale features that correlate with the seismic velocity structures. However, it is well appreciated that, because of the strong influence of focusing effects, global attenuation models are strongly damped and that they may underestimate the peak-to-peak variation in attenuation within various regions. It is therefore difficult to determine whether the elastic and anelastic seismic structures in the shallow mantle have a common physical origin.

[5] In this study we analyze attenuation in the upper mantle using broadband teleseismic (epicentral distance = 30°–85°) *P* wave spectra of deep earthquakes. We focus on the North American continent. Here resolution is relatively high because of the dense station coverage offered by the various regional seismic networks. Moreover, we expect large variations in attenuation in North America due to its diverse tectonic terrains, facilitating a comparison of models obtained from a variety of data types.

[6] We compare our results to the most recent global surface wave attenuation model [*Dalton et al.*, 2008] and an attenuation model inferred from a thermal conversion of a regional shear velocity model [*Goes and van der Lee*, 2002]. This allows us to place our results in a global context, to determine the compatibility of the body wave and surface wave attenuation constraints, and to evaluate whether a thermal interpretation of shear velocity variation and attenuation is justified.

2. Seismic Wave Attenuation in North America

[7] The Rocky Mountain Front divides North America into tectonic western North America (TNA) and stable eastern North America (SNA). TNA is associated with current extension in the Basin and Range, subduction under Oregon and Washington continued to transform motion in California, and volcanism in Yellowstone and western Rocky Mountain front [*Burchfiel et al.*, 1992; *Humphreys and Coblentz*, 2007]. In contrast, the most recent tectonic event in SNA is related to the Appalachian orogeny (330–265 Ma) [*Dallmeyer et al.*, 1986; *Secor et al.*, 1986].

[8] Geophysical studies of the upper mantle and the lithosphere indicate that a structural divide between TNA and SNA persists in the mantle. High surface heat flow, low-amplitude magnetic anomalies, and a negative long wavelength Bouguer gravity in TNA indicate that the mantle below TNA is hot while low surface heat flow and short wavelength magnetic and gravity anomalies indicate a cool lithosphere mantle below SNA [*Morgan and Gosnold*, 1989]. Studies of body wave traveltime [*Grand and Helmberger*, 1984; *Melbourne and Helmberger*, 1998] and surface wave dispersion [*Van der Lee and Nolet*, 1997; *Marone and Romanowicz*, 2007] show that the shear velocity in the upper mantle beneath SNA and TNA differs by as much as 15–20%.

[9] A large number of studies have provided constraints on the attenuation structure in North America, including analyses of short-period amplitude anomalies [*Cleary*, 1967; *Booth et al.*, 1974; *Butler and Ruff*, 1980; *Der et al.*, 1982; *Butler*, 1984], spectral ratio variations [*Solomon and Toksöz*, 1970; *Der and McElfresh*, 1976, 1977; *Der et al.*, 1982], *Lg* coda waves [*Baqer and Mitchell*, 1998], and *ScS* multiples [*Lay and Wallace*, 1988]. The studies show a common first-order pattern of a highly attenuating TNA and low-attenuation SNA. In addition, the regional studies indicate that smaller-scale (<1000 km) variations of attenuation can be as large as the continental-scale contrast between TNA and SNA. *Lay and Wallace* [1988], for example, suggest that shear wave attenuation in the upper mantle beneath the Basin and Range, a region with extremely high heat flow, is as strong as attenuation beneath active mid-ocean ridge spreading centers and that attenuation beneath the Pacific Northwest is comparable to attenuation within western Pacific subduction zones.

3. *P* Wave Spectral Analysis

[10] In addition to the geometric spreading of wavefronts, seismic waves are attenuated by anelastic energy dissipation and scattering. The efficiency of wave propagation is commonly expressed by the quality factor Q. Its inverse, Q^{-1}, quantifies wave attenuation. Q^{-1} is defined as

$$Q^{-1} = \Delta E / 2\pi E_{\max}, \tag{1}$$

where ΔE is the energy lost per cycle and $E_{\max}$ is the maximum elastic energy contained in a cycle.

[11] The attenuation of teleseismic body waves is defined by the attenuation parameter t^*. The t^* parameter is a station-specific observable that represents the total body wave traveltime divided by Q along the raypath [*Stein and Wysession*, 2003]:

$$t^* = \int_{ray} \frac{1}{V(r)Q(r)} ds. \tag{2}$$

Typically, $t_P^* = 1$ s for teleseismic *P* waves and $t_S^* = 4$ s for teleseismic *S* waves [*Cormier*, 1982]. These values vary little with epicentral distance [*Booth et al.*, 1974] suggesting that body waves are attenuated primarily in the upper mantle. This observation is consistent with one-dimensional profiles derived from long-period surface waves and normal modes [*Dziewonski and Anderson*, 1981; *Durek and Ekström*, 1996] which show that Q values in the upper mantle are an order of magnitude lower than in the lower mantle.

[12] In this study, we measure t_P^* from teleseismic *P* wave spectra. t_P^* encompasses multiple effects: intrinsic attenuation, crustal amplification, focusing and defocusing, and local scattering in the upper mantle under the receiver. Probably, each of these factors is equally important given the large scatter seen in measurements of t_P^*. To isolate the contribution of intrinsic attenuation to t_P^*, we rely on a large and redundant set of *P* wave spectra for earthquake/receiver combinations over a wide range of azimuths.

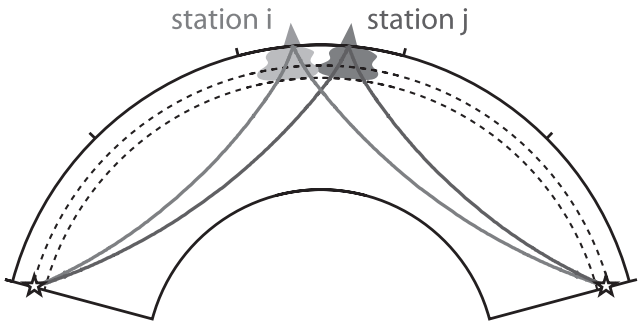

Figure 1. Geometrical raypaths of *P* waves propagating from deep earthquake sources (stars) to stations at teleseismic distances (triangles).

3.1. Teleseismic *P* Wave Spectra

[13] We follow the classical approach developed by *Teng* [1968] and *Solomon and Toksöz* [1970]. We write the spectrum $O(f)$ of a teleseismic seismogram as

$$O(f) = S(f)\exp\left(-\pi f t_P^*\right), \tag{3}$$

where $S(f)$ is the earthquake source spectrum and $\exp(-\pi f t_P^*)$ is the attenuation function. The logarithm of the ratio R_{ij} between the spectrum O_i and O_j at stations i and j is expected to change linearly with frequency f for the same earthquake:

$$\ln R_{ij}(f) = -\pi f \Delta {t_P}^*_{ij}. \tag{4}$$

Δt_P^* reflect differences in *P* wave attenuation in the upper mantle beneath regional network stations. We expect the influence of the lower mantle on Δt_P^* to be small because attenuation in the lower mantle is relatively weak and *P* waves have similar lower mantle propagation paths for nearby stations (Figure 1). One of the benefits of using the spectral ratio over using the amplitude ratio to infer the variation in t_P^* is that the shapes of spectra are not as sensitive to other elastic effects such as crustal amplification, azimuthal variation, focusing, and local scattering near the source as they are to t_P^* while the amplitudes of body waves are severely affected by local focusing [*Der et al.*, 1982].

[14] We restrict our analysis to teleseismic *P* wave recordings of deep (focal depths > 200 km) earthquakes. *P* signals for deep earthquakes have relatively short durations without significant directivity [*Houston and Vidale*, 1994]. Moreover, they are not complicated by surface reflections (i.e., *pP* and *sP*) nor attenuated by the uppermost mantle in the source region. For epicentral distances larger than 30° and smaller than 85°, *P* waves turn below the 660 km discontinuity and above the heterogeneous D″ region, where vertical velocity gradients are well understood. However, since teleseismic *P* waves propagate steeply through the upper mantle, Δt_P^* does not constrain depth variation of attenuation.

[15] We select our recordings from 378 stations (Figure 2). These include Global Seismic Network and GEOSCOPE stations in the U.S. and Canada and regional network stations from the Canadian National Seismic Network (CNSN), the United States National Seismic Network (USNSN), TriNet [*Kanamori et al.*, 1997], the Berkeley Digital Seismic Network (BDSN) [*Romanowicz et al.*, 1993], NARS-Baja [*Trampert et al.*, 2003], and broadband PASSCAL arrays that have been archived at the IRIS Data Management Center. *P* waves on broadband (10 samples per second) vertical component velocity seismograms are corrected for the instrument response and high-pass filtered with a corner frequency of 120 s to reduce long-period noise. By visual inspection, we select the highest-quality recordings of *P* waves with signal-to-noise ratios of at least 20, low-amplitude coda, and impulsive onsets and we determine time windows to ensure that the same features of *P* waveforms are analyzed. *P* wave spectra are estimated by multiple-taper spectral analysis [*Lees and Park*, 1995] and spectral ratios ln*R* are measured up to 1 Hz. The use of multiple-tapers produces smoother spectra and, hence, more robust estimates of ln*R*. However, after experimentation with single and multiple tapers we observe that the spatial distribution of t_P^* depends little on the choice of the taper.

[16] Figure 3 shows representative examples of spectral ratios and the measurement variability in Δt_P^* for ten deep earthquakes in South America recorded at stations CCM (Cathedral Cave, Missouri) and ANMO (Albuquerque, New Mexico). It demonstrates that, for nearly all earthquakes, the *P* wave signals at ANMO (which is located in TNA) are depleted in high frequencies compared to the *P* wave signals recorded at CCM (which is located in SNA). For each waveform pair, the spectral ratio ln*R* increases with increasing frequency and, hence, values for Δt_P^* ($t_{P\,\mathrm{CCM}}^* - t_{P\,\mathrm{ANMO}}^*$) are negative. This suggests that *P* waves propagating to ANMO are more attenuated. However, inferred values for Δt_P^* vary between −0.24 s and −1.09 s, more than measurement errors in Δt_P^* (±0.05–0.37 s). The variable Δt_P^* reflects the complex (nonlinear) character of ln*R*, especially at frequencies larger than 0.8 Hz, which we attribute to receiver effects. In general, we obtain

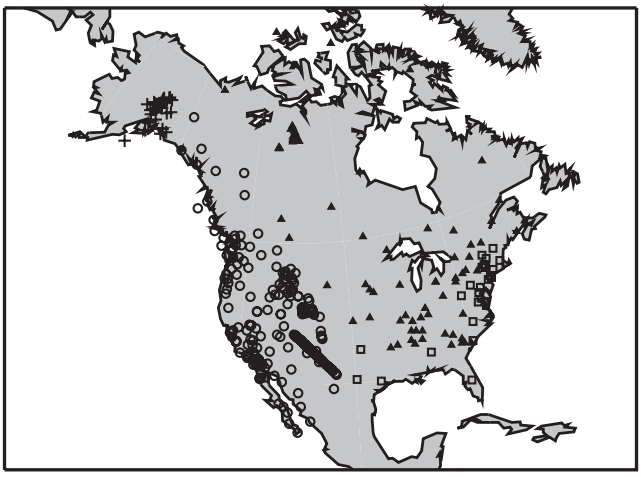

Figure 2. Open circles, closed triangles, open squares, and crosses indicate the locations of the 378 seismic stations used in this study. These stations are located in, respectively, SNA, TNA, the off-platform region, and subduction zone in southern Alaska.

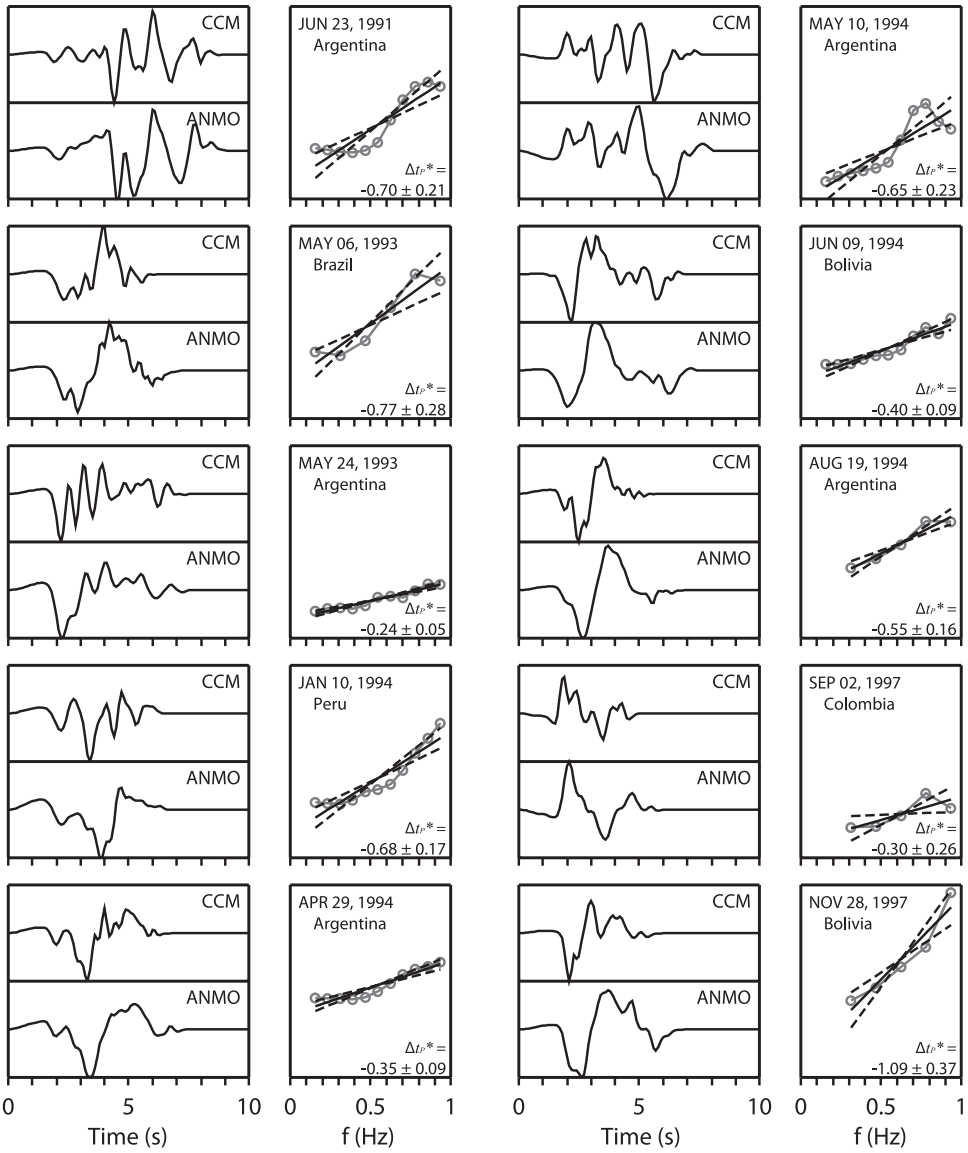

Figure 3. Selected measurements of Δt_P^* between stations CCM (Cathedral Caves, MO) and ANMO (Albuquerque, NM) for ten deep earthquakes in South America. (left) Vertical component velocity waveforms. Trace windows are manually determined such that seismograms for the same event contain the same features of P wave arrivals. (right) Natural logarithm of spectral ratios $\ln R(f)$ (gray lines with circles), best fitting lines to $\ln R$ (black solid lines), and lines with slopes that bracket the 95% certainty of the slope (black dashed lines). Δt_P^* measurements and their uncertainties are in seconds.

the most accurate measurements of Δt_P^* (i.e., measurements with uncertainties lower than 2σ) for P waves with simple waveforms composed of a single upswing and downswing) and shortest durations. Presumably, these measurements better quantify the integrated effects of intrinsic attenuation on P wave spectra.

[17] We observe significant variability of Δt_P^* for most station pairs (Figure 4). While absolute Δt_P^* values are larger than 0.1 s for about 75% of the measurements, the measurement uncertainty peaks at around 0.1 s. Thus, to constrain Δt_P^* we must rely on data redundancy and multiple measurements for earthquakes at different azimuths. Therefore we collect a data set of more than 63,000 spectral ratios using stations for which we have at least two events.

3.2. Least Squares Inversion

[18] To estimate t_P^* for each station, we solve a set of linear equations. First, the measurements of the slopes of the best fitting lines to $\ln R_{ij}$ provide estimates of the t_P^* difference ($\Delta t_{P\,k}^*$) between stations i and j:

$$w_k^1\left(t_P{}^*{}_i - t_P{}^*{}_j\right) = w_k^1 \Delta t_P{}^*{}_k. \tag{5}$$

Here w_k^1 is a weight factor

$$w_k^1 = \exp\left[-(\varepsilon_k/\varepsilon_0)^2\right] \exp\left[-(\Delta_k/\Delta_0)^2\right], \tag{6}$$

which includes factors determined by the 2σ uncertainty in the $\Delta t_{P\,k}^*$ measurement (ε_k) and the interstation distance

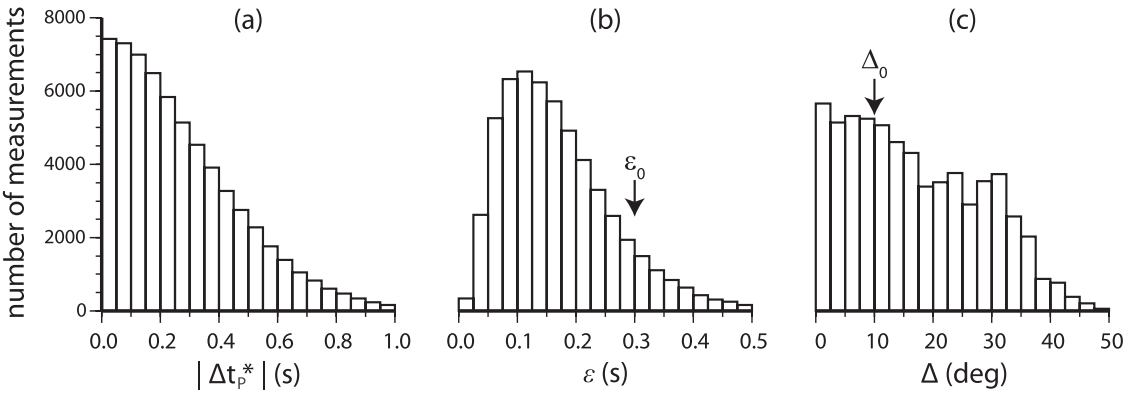

Figure 4. (a) Distribution of $|\Delta t_P^*|$. (b) Distribution of 95% confidence ranges of Δt_P^*. Reference value $\varepsilon_0 = 0.3$ s is chosen. (c) Interstation distance distribution of station pairs used in this study. Reference value $\Delta_0 = 10^\circ$ is chosen.

(Δ_k). The first factor in (6) reduces the weight of measurements Δt_P^* with the highest 2σ uncertainty. The second factor reduces the weight of measurements of Δt_P^* for stations that are separated most and for which the effects of variable attenuation in the lower mantle may be greatest. We choose reference values $\varepsilon_0 = 0.3$ s (Figure 4b) and $\Delta_0 = 10^\circ$ (Figure 4c) so that measurements with uncertainties larger than 0.3 s and measurements for which the station separations are more than 10° have weights that are reduced by at least $1/e$. The inversion results change little when ε_0 is larger than 0.3 s and when Δ_0 is larger than 10° because $\Delta t_{P\ k}^*$ for the same pair of stations have, in general, the same signs.

[19] Second, we impose that the average value of t_P^* is zero:

$$\sum_{n=1}^{378} t_{P\,n}^* = 0, \tag{7}$$

since the differential t_P^* measurements do not constrain the absolute value of t_P^*. Thus, in our maps, only the variation in t_P^* is estimated.

[20] Third, we impose smoothness constraints by penalizing t_P^* differences for closely located stations:

$$w_k^2\left(t_P{}^*{}_i - t_P{}^*{}_j\right) = 0. \tag{8}$$

The factor

$$w_k^2 = \exp\left[-\left(\Delta_k/\Delta_R\right)^2\right] \tag{9}$$

is largest when the angular distance Δ_k between stations i and j is smallest. In section 4.1, we experiment with values for the reference distance Δ_R by examining data misfit reduction and model norm.

[21] Equations (5), (7), and (8) can be written in matrix form as

$$\mathbf{Gm} = \mathbf{d}, \tag{10}$$

where $\mathbf{m}$ is the model vector composed of t_P^* for 378 stations:

$$\mathbf{m} = \left(t_P{}^*{}_1, t_P{}^*{}_2, t_P{}^*{}_3, \cdots, t_P{}^*{}_{378}\right). \tag{11}$$

We solve (10) by least squares inversion.

4. t_P^* Structure

4.1. Effect of Smoothing

[22] In order to determine the effects of the smoothing parameter Δ_R, we determine model norm $(\mathbf{m}/\mathbf{m}_0)^2$, misfit reduction $1 - ((\mathbf{Gm} - \mathbf{d})/\mathbf{d})^2$ (Figure 5), and t_P^* as a function of Δ_R (Figure 6). Figure 5 illustrates the trade-off between model norm and misfit reduction. For low values of Δ_R, the model norm is high ($|t_P^*|$ values are relatively large) and misfit reduction is highest (i.e., data fit is best). For increasing Δ_R, both model norm and misfit reduction decrease and the t_P^* contrast between TNA and SNA emerges as the predominant signal. We choose $\Delta_R = 3^\circ$ as the preferred smoothness value as we suppress the strong variations in t_P^* for nearby stations within the western US while maintaining coherent variations in t_P^* within TNA and SNA (e.g., relatively high t_P^* around the Appalachian) for which we may seek geophysical explanations. However,

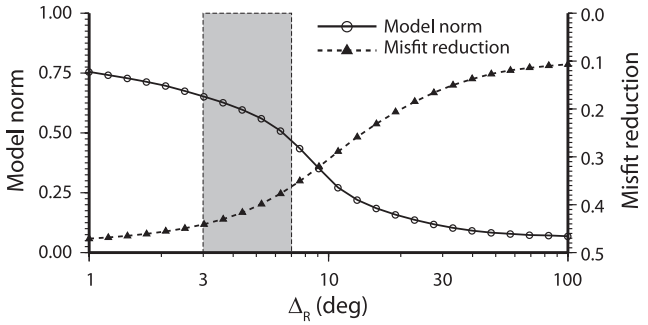

Figure 5. Trade-off curves for the model norm (solid line with circles) and the misfit reduction (dashed line with triangles) as a function of Δ_R. Circles and triangles are calculated data points of the model norm and the misfit reduction, respectively. Values of Δ_R in the shaded region ($\Delta_R = 3$–7°) are preferred values.

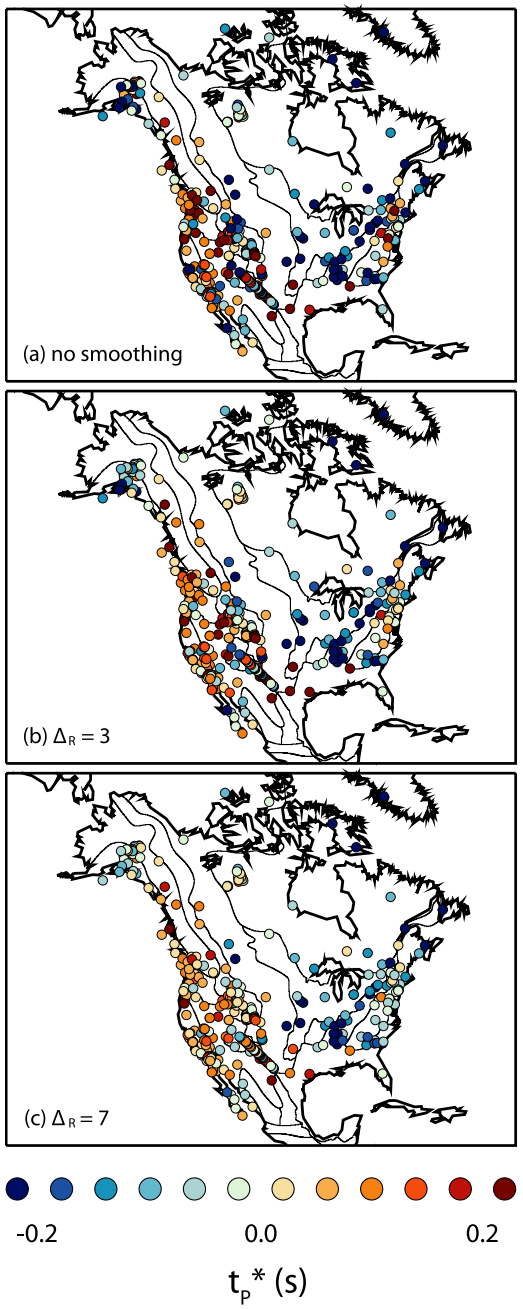

Figure 6. Maps of t_P^* resolved with varying smoothing parameters Δ_R. (a) No smoothing is imposed. (b) $\Delta_R = 3°$. (c) $\Delta_R = 7°$.

an acceptable misfit reduction is obtained for Δ_R as high as 7°.

4.2. Variation in t_P^*

[23] Our preferred map of t_P^* variation (Figure 6b) shows both a simple regional trend and small-scale variations. The characteristic dichotomy of SNA and TNA is reflected in predominantly low t_P^* values for stations in SNA, including the Canadian Shield, Midcontinent, Grenville Province, and most of the Great Plains, while high values of t_P^* are observed in TNA. We illustrate the regional variation in t_P^* further by dividing the stations into four groups for distinct terrains in North America (Figure 7). The main variations can be associated with regional tectonic settings. Low t_P^* values for stations in SNA and high t_P^* values for stations in TNA are shown clearly in Figures 7a and 7b, respectively. On average, the difference in t_P^* between SNA and TNA is 0.23 s when no smoothing is applied and is 0.16 s if Δ_R is increased to 7°.

[24] Smaller-scale (<1000 km) variations of t_P^* are embedded within this large-scale trend and they are as strong as the bimodal TNA/SNA variation. We can readily recognize these variations in individual spectral ratio measurements. Compared to the predominant low t_P^* values at stations in SNA (Figure 7a), relatively high values for t_P^* are resolved for stations around the Appalachians and Gulf coast off the stable platform (Figure 7c), where mantle shear and P velocities are also relatively low. Low t_P^* are found under southern Alaska and around Baja California (Figure 7d), probably associated with ongoing subduction in Alaska, while t_P^* are relatively high in the rest of western North America (Figure 7b).

5. Comparison With Other Studies

[25] The first-order pattern of high t_P^* in TNA and low t_P^* in SNA is consistent with previous studies of short-period amplitude anomalies [*Cleary*, 1967; *Booth et al.*, 1974; *Der et al.*, 1982; *Butler*, 1984], spectral ratio variations [*Solomon and Toksöz*, 1970; *Der and McElfresh*, 1976, 1977; *Der et al.*, 1982], *Lg* coda waves [*Baqer and Mitchell*, 1998], and regional Rayleigh waves [*Mitchell*, 1975]. The contrast in t_P^* of 0.2 s between SNA and TNA is consistent with that inferred by *Der et al.* [1982] who studied P wave spectra at frequencies up to 4 Hz. From P wave amplitudes, values of Δt_P^* larger than 0.4 s have been reported by *Solomon and Toksöz* [1970] and *Lay and Helmberger* [1981]. In contrast, the recent study by *Lawrence et al.* [2006] suggests that there is no significant large-scale variation in t_P^* across North America. This observation is clearly inconsistent with our study. We speculate that the discrepancy is due to the fact that t_P^* variation may be difficult to detect in spectral ratios within the low frequency band (f < 0.1 Hz) that *Lawrence et al.* [2006] use.

[26] *Lay and Wallace* [1988] resolve strong Q_S variations within western North America using *ScS* multiples. Averaged over the upper 400 km of the mantle, they suggest that $Q_S = 25$ beneath the Basin and Range and $Q_S \geq 1000$ beneath the Pacific Northwest. This contrast would imply t_P^* variations of about 0.4 s, a factor of 2 higher than what we observe. This discrepancy that may partially be due to a strong D″ influence on *ScS* attenuation measurements. Strong (frequency-dependent) wave attenuation beneath the Basin and Range is also inferred from regional *Lg* wave [*Chavez and Priestley*, 1986; *Benz et al.*, 1997] and Rayleigh wave studies [*Hwang and Mitchell*, 1987].

[27] The main patterns in our t_P^* maps, including those at regional scale, are similar to those found in surface heat flow (Figure 8d). The low heat flow in southeastern U.S. does not correlate with the high t_P^* anomaly in this region. However, *Artemieva et al.* [2000] did infer higher lithospheric temperatures for the southeastern U.S. than in the SNA interior by reevaluation of heat flow data that takes

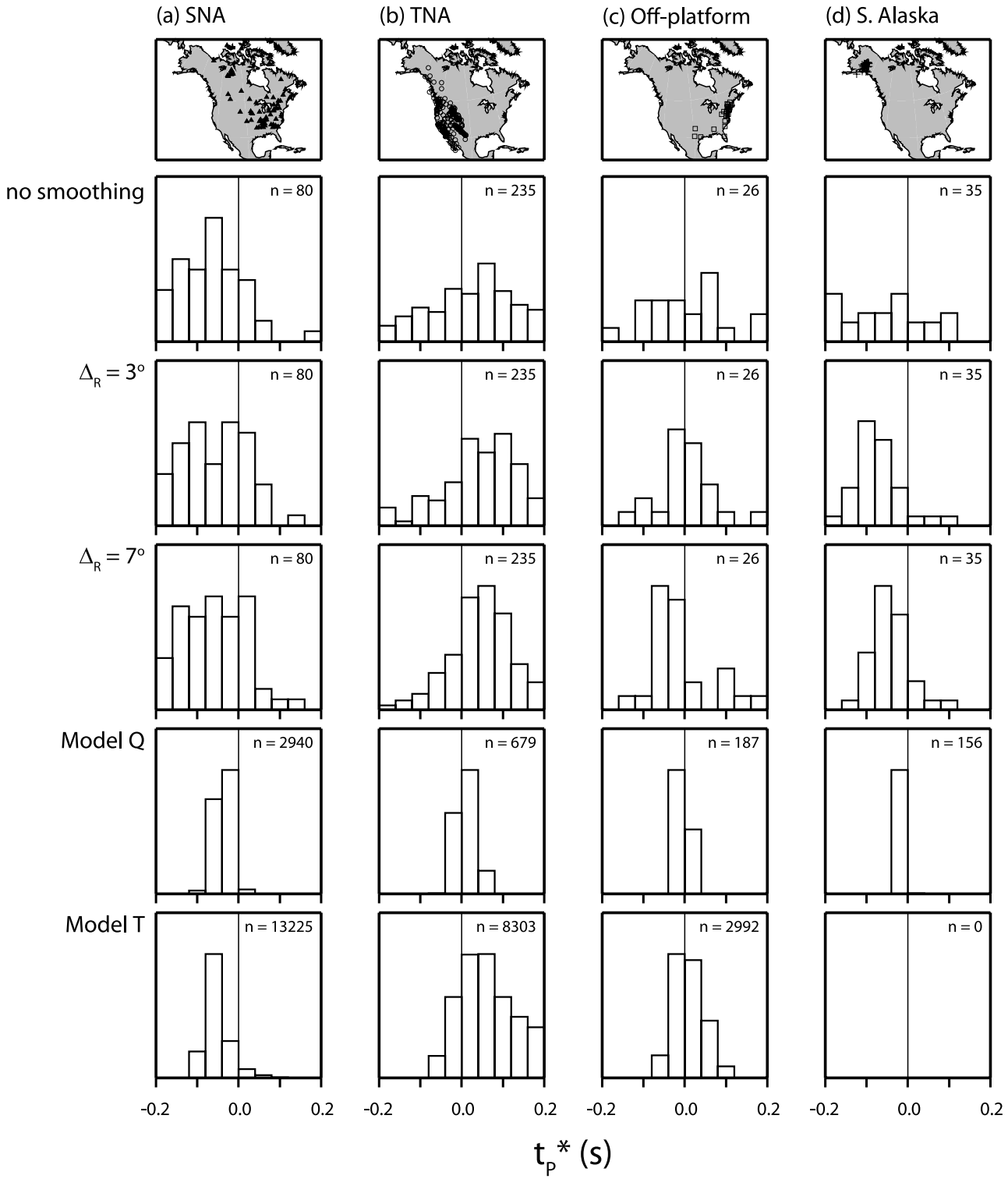

Figure 7. Distributions of t_P^* (this article), t_Q^* (from model Q: global surface Q tomography [*Dalton et al.*, 2008]), and t_T^* (from model T: regional Q_S from temperature estimates [*Goes and van der Lee*, 2002]) for stations in (a) SNA, (b) TNA, (c) off-platform region, and (d) subduction zone in southern Alaska. n represents the total number of data points used to produce each distribution diagrams.

into account the thermal properties of the region's crust. The similarity of surface heat flow and t_P^* implies that thermal structure affects intrinsic attenuation to a significant extent at shallow mantle depth.

[28] Next, we make a more detailed comparison with two recent attenuation models based on surface wave analyses. We refer to these models as models Q and T. Model Q is the global model QRFSI12 by *Dalton et al.* [2008]. Model T is

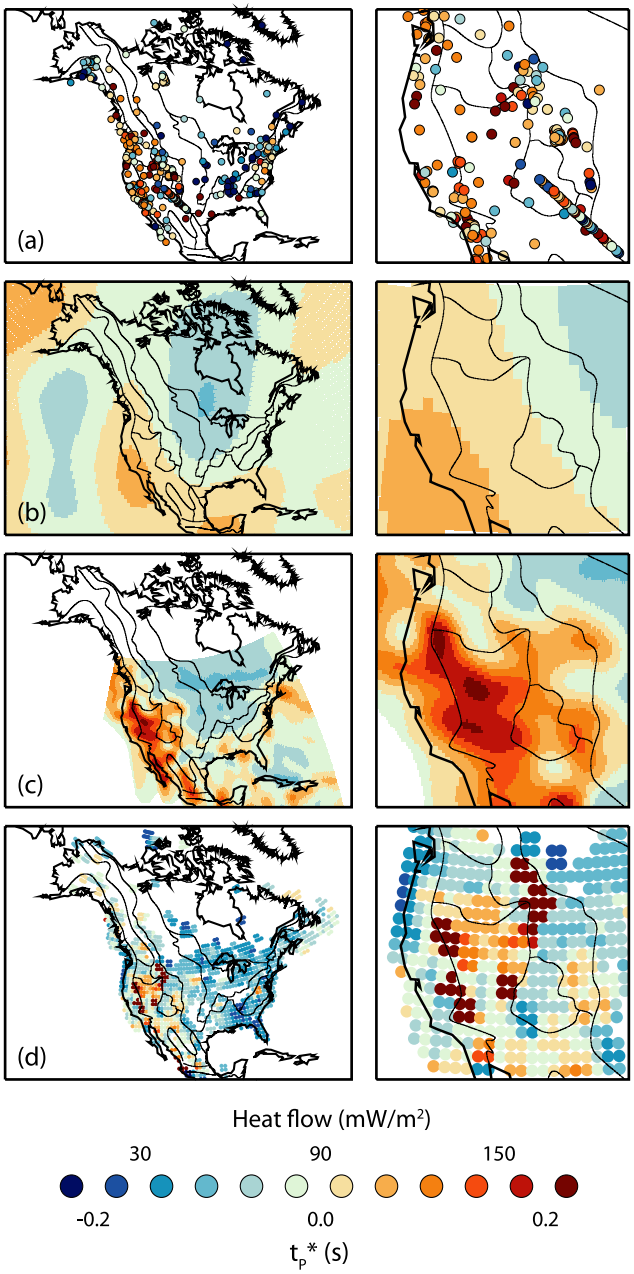

Figure 8. (a) Variation of t_P^* for $\Delta_R = 3°$. (b) Variation of t_Q^* (from model Q: global surface Q tomography [*Dalton et al.*, 2008]). (c) Variation of t_T^* (from model T: regional Q_S from temperature estimates [*Goes and van der Lee*, 2002]). (d) Variation of cap-averaged heat flow data from *Pollack et al.* [1993]. (left) Variations in North America. (right) Variations within TNA.

derived from the regional S velocity model for NA00 [*Van der Lee*, 2002] for North America by converting shear velocity to temperature [*Goes and van der Lee*, 2002]. The conversion accounts for both elastic and anelastic sensitivity of the seismic waves to temperature and as a result yields an accompanying anelasticity model.

[29] We denote predicted values of t_P^* for model Q as t_Q^*, using the subscript "Q" to emphasize that t_P^* values are computed using a Q_S model for the mantle. The predicted t_P^* for model T are denoted as t_T^*, using a subscript "T" to indicate that we employ a temperature conversion to infer t_P^* from a tomographically derived shear velocity model.

[30] The comparison with model Q (and t_Q^*) will help us gain insight into the compatibility of attenuation inferred from P wave spectra and long-period surface wave amplitudes. The comparison with model T (and t_T^*) will enable us to evaluate the similarity of regional-scale variations in t_P^* and shear velocity, and whether interpreting North American shear wave structure as being dominantly thermally controlled is compatible with independent constraints on attenuation. Figure 8 compares the t_P^* map from Figure 6b to predicted values of t_P^* across North America for models Q (t_Q^*) and T (t_T^*). The distribution of t_P^*, t_Q^*, and t_T^* is shown in Figure 7.

5.1. Model Q: Global Surface Wave Q Tomography

5.1.1. Model Q Background

[31] Model QRFSI12 [*Dalton et al.*, 2008] is the most recent global Q_S model based on surface wave amplitudes. QRFSI12 has been derived using more than 30,000 Rayleigh wave amplitudes measurements. These amplitudes have been corrected for the effects of surface wave focusing and inverted simultaneously for three-dimensional attenuation (Q_S) and correction factors for the source and receiver. Lateral variations of Q_S in QRFSI12 are parameterized using spherical harmonics up to degree 12. The shortest wavelength variations are therefore about 3000 km which limits a comparison to continental-scale variations. We convert Q_S from QRFSI12 to Q_P using $Q_P = {}^3/_4(V_P/V_S)^2 Q_S$, assuming that attenuation in bulk is negligible, and we adopt V_P and V_S velocities from the PREM model [*Dziewonski and Anderson*, 1981].

[32] We calculate t_Q^* by integrating along a P wave raypath for an epicentral distance of 70° through the upper 370 km of the mantle using (2). We assume that Q_P varies only with depth, because lateral variations in Q_P are smooth and teleseismic P wave propagate steeply through the uppermost mantle.

5.1.2. Comparison Between t_Q^* and t_P^*

[33] The t_Q^* variation (Figure 8b) is, as expected, smooth given the relatively coarse lateral parameterization of QRFSI12. The contrast between SNA and TNA, a regional variation that is at the limit of global resolution in QRFSI12, is well reproduced in t_Q^* and correlates well with t_P^*, with a correlation coefficient of 0.30, on a point by point basis. The correlation coefficient increases to 0.38 and to 0.40 for $\Delta_R = 3°$ and $\Delta_R = 7°$, respectively.

[34] The peak-to-peak variation in t_Q^* is a factor of 6 smaller than in the preferred t_P^* ($\Delta_R = 3°$). Even for stronger damped distributions of t_P^* ($\Delta_R = 12°$) for which the lateral resolutions of t_Q^* and t_P^* are roughly equal, the amplitude in t_Q^* is still a factor of 2.2 smaller. We attribute the amplitude mismatch to the relatively long wavelength parameterization and strong damping used in constructing QRFSI12.

5.2. Model T: Regional Q_S From Temperature Estimates

5.2.1. Model T Background

[35] Model T is a regional Q_S model derived from a purely thermal interpretation [*Goes and van der Lee*, 2002]

of shear velocity model NA00 [*Van der Lee*, 2002], assuming a constant pyrolitic composition. Taking into account that temperature variations affect both elastic and anelastic seismic structure, the conversion yields all elastic constants, density, and Q_S and Q_P for the temperature structure inferred from V_S. Because of the exponential dependence of anelasticity on temperature, even strong low-velocity anomalies generally translate into subsolidus temperatures that are compatible with temperatures derived from an independent V_P model and surface heat flow [*Goes and van der Lee*, 2002].

[36] The temperature-velocity calculations were slightly updated from those used by *Goes and van der Lee* [2002] to make them more suitable for depths between 200 km and 400 km. We employ a finite, rather than infinite, strain equation of state that includes the effect of phase transformations within the pyrolitic mantle, as in the study by *Goes et al.* [2005]. We use a temperature and depth-dependent anelasticity formulation: $Q_S(T, P) = Q_0 \exp[gT_m(P)/T]$, where Q_0 is set to $0.1 \cdot \omega^{0.15}$, ω is frequency, g is a constant scaling factor set to 40, T_m is the peridotite solidus, and T is absolute temperature. This is an empirical approximation of the common Arrhenius-type expression $Q_S(T, P) = Q_0 \cdot \exp[(E^* + PV^*)/T]$, where E^* and V^* are activation energy and volume, respectively [*Karato and Spetzler*, 1990]. Using the scaled homologous temperature, T/T_m, is a way of parameterizing the plausible decrease of V^* with depth [e.g., *Yamazaki and Karato*, 2001]. A constant V^* yields negative upper mantle Q_S depth gradients below the asthenosphere. At depths down to about 200 km, the model is similar to the average Q model Q_1 (with $E^* = 500$ kJ/mole and $V^* = 20$ m^3/mole) used by *Goes and van der Lee* [2002]. Bulk Q is kept constant at a value of 1000. The updated procedure gives temperatures that are, within a few tens of degrees, i.e., within the uncertainties due to uncertainties in the mineral parameters, identical to those from *Goes and van der Lee* [2002].

5.2.2. Comparison Between t_T^* and t_P^*

[37] Because of the relatively high lateral resolution of NA00, t_T^* (Figure 8c) shows more variability than t_Q^*. In addition to the bimodal SNA-TNA variation, t_T^* includes high values below the Appalachians and Gulf Coast, and lower values under the Colorado Plateau that are also observed in t_P^*. This indicates that not only the continental-scale pattern but some of the t_P^* features that are coherent on a 2° scale may be the result of intrinsic attenuation. However, the point-by-point correlation coefficient between t_P^* and t_T^* of 0.23 is relatively low and thus shows that many of the high and low shear velocity anomalies do not correspond to high and low Q anomalies.

[38] The amplitude variation in t_T^* is in good agreement with the variation of t_P^*. The similar amplitudes of t_P^* and t_T^* indicate that the assumptions underlying the conversion of shear velocity variation to Q_P are reasonable. Q_P in model T varies over at least 6 orders of magnitude from essentially infinite under the North American shield, to minimum values of 40 (Q_S of 17) around 70 km depth below the western U.S. Higher Q_P (and hence higher Q_S) values within the western US would reduce t_T^* values which already somewhat underestimate t_P^*.

[39] Thus Q values below the western US appear to be very low. Similarly low Q values have been invoked below mid-ocean ridges in models that reconcile oceanic lithospheric cooling models and sub-oceanic surface wave velocities [*Faul and Jackson*, 2005; *Priestley and McKenzie*, 2006]. These models self-consistently generate a low-velocity zone without requiring significant amounts of partial melt. However, surface wave analyses from data of the East Pacific Rise RIDGE experiment find minimum Qs values no lower than 80 below the ridge [*Yang et al.*, 2007]. To reconcile very low seismic velocities and moderately low Qs values, the authors propose the presence of melt which does not attenuate substantially in the seismic frequency band but lowers seismic velocities due to elastic effects.

[40] We find that for the western U.S., where mantle seismic velocities are, over 1000 km scales, as low as at mid-ocean ridges, measured t_P^* are matched well with very low Q values. Such low Q values can be purely thermal (as was assumed in their derivation), but may also be partially controlled by water content. *Dixon et al.* [2004] has proposed that the western U.S. subcrustal mantle is both hot and wet. As the seismic effect of water at shallow mantle depths is most likely predominantly anelastic, water affects seismic velocities and Q simultaneously, and cannot be distinguished from purely thermal effects without independent temperature data [*Karato*, 1993]. The relatively large scatter in surface heat flow data and uncertainties in their extrapolation to temperature at depth does not preclude that part of the seismic structure is controlled by variations in water content [*Dixon et al.*, 2004]. In any case, the variable seismic velocities in the North American upper mantle seismic structure are linked to strong attenuation variations. This strongly suggests that these seismic signatures are caused by variations in temperature and water content, and probably not by composition and melt.

6. Conclusions

[41] We have inverted about 63,000 measurements of the spectral ratio of broadband (from one over signal length to 1 Hz) P waves generated by deep (focal depths > 200 km) earthquakes and recorded at 378 stations in North America. This large data set provides better constrained and more densely distributed information on uppermost mantle P wave attenuation below the continent than has been previously available.

[42] The pattern of t_P^* shows a systematic contrast between tectonic North America (TNA) and stable North America (SNA). t_P^* is relatively high in TNA and low in SNA consistent with high and low P wave attenuation in the upper mantle beneath TNA and SNA, respectively. This general pattern has been observed before in the US; improved data coverage in Canada confirms that the continental-scale t_P^* pattern matches very well with the age of geological terrains and the seismic, heat flow, gravity, and magnetic variations across North America. The variation of t_P^* of 0.2 s between TNA and SNA is compatible with previous estimates.

[43] We resolve regional variations in t_P^* which correlate with tectonics: relatively low t_P^* is associated with currently active subduction below Alaska. Relatively high t_P^* is found in SNA below the Appalachians and the Gulf Coast.

[44] The consistency between patterns on the scale of around 200–500 km and tectonics suggests that the ob-

served variations in t_P^* are predominantly due to intrinsic attenuation. The similar patterns in our t_P^* and predicted values for global attenuation model QRFSI12 [*Dalton et al.*, 2008] based on Rayleigh waves, which samples the upper mantle in a fundamentally different manner than teleseismic *P* waves, confirm this further. Compatibility with the t_P^* computed for attenuation estimated via a thermal interpretation of shear wave velocity anomalies in regional *Vs* model NA00, illustrates that variations in seismic velocity are predominantly due to physical effects with a strong attenuation signature, most likely temperature or a combination of temperature and water content.

[45] **Acknowledgments.** Data have been provided by the IRIS/DMC, the GEOSCOPE Data Center, the Geological Survey of Canada, the Southern California Seismic Network (SCSN) Data Center operated by Caltech and USGS, and the Northern California Earthquake Data Center (NCEDC), a joint project of the University of California Berkeley Seismological Laboratory (BSL) and the USGS. Figures are produced by GMT (Generic Mapping Tools) software. We thank Colleen Dalton for providing us with her *Q* model and for giving advice on model interpretation. We thank Jonathan Lees for providing us with the MTM (Multi-Taper Spectral Analysis Methods) software. Constructive comments by two anonymous reviewers and the Associate Editor helped us improve the article. This research has been supported by NSF grant EAR-0609763.

References

Artemieva, I. M., W. D. Mooney, and N. H. Sleep (2000), Plate motions and the destruction of lithospheric keels, *Eos Trans. AGU*, *81*, 1177.

Baqer, S., and B. J. Mitchell (1998), Regional variation of Lg coda *Q* in the continental United States and its relation to crustal structure and evolution, *Pure Appl. Geophys.*, *153*, 613–638.

Benz, H. M., A. D. Frankel, and D. M. Boore (1997), Regional Lg attenuation for the continental United States, *Bull. Seismol. Soc. Am.*, *87*, 606–619.

Bhattacharyya, J., G. Masters, and P. M. Shearer (1996), Global lateral variations of shear wave attenuation in the upper mantle, *J. Geophys. Res.*, *101*, 22,273–22,289.

Billien, M., J.-J. Leveque, and J. Trampert (2000), Global maps of Rayleigh wave attenuation for periods between 40 and 150 seconds, *Geophys. Res. Lett.*, *27*, 3619–3622.

Booth, D. C., P. D. Marshall, and J. B. Young (1974), Long and short period P-wave amplitudes from earthquakes in the range 0 degrees–114 degrees, *Geophys. J. R. Astron. Soc.*, *39*, 523–537.

Burchfiel, B. C., D. S. Cowan, and G. A. Davis (1992), Tectonic overview of the Cordilleran orogen in the western United States, in *The Geology of North America*, vol. G-3, *The Cordilleran Orogen: Conterminous U.S.*, edited by B. C. Burchfiel, P. W. Lipman, and M. L. Zoback, pp. 407–479, Geol. Soc. of Am., Boulder, Colo.

Butler, R. (1984), Azimuth, energy, *Q*, and temperature: Variations on P wave amplitudes in the United States, *Rev. Geophys.*, *22*, 1–36.

Butler, R., and L. Ruff (1980), Teleseismic short-period amplitudes; source and receiver variations, *Bull. Seismol. Soc. Am.*, *70*, 831–850.

Chavez, D. E., and K. F. Priestley (1986), Measurement of frequency dependent Lg attenuation in the Great Basin, *Geophys. Res. Lett.*, *13*, 551–554.

Cleary, J. (1967), Analysis of the amplitudes of short-period P waves recorded by long range seismic measurements stations in the distance range 30 degrees to 102 degrees, *J. Geophys. Res.*, *72*, 4705–4712.

Cormier, V. F. (1982), The effect of attenuation on seismic body waves, *Bull. Seismol. Soc. Am.*, *72, Part B*, S143–S173.

Dallmeyer, R. D., J. E. Wright, D. T. Secor Jr., and A. W. Snoke (1986), Character of the Alleghanian Orogeny in the Southern Appalachians: Part II. Geochronological constraints on the tectonothermal evolution of the eastern Piedmont in South Carolina, *Geol. Soc. Am. Bull.*, *97*, 1329–1344.

Dalton, C. A., and G. Ekström (2006), Global models of surface wave attenuation, *J. Geophys. Res.*, *111*, B05317, doi:10.1029/2005JB003997.

Dalton, C. A., G. Ekström, and A. M. Dziewoński (2008), The global attenuation structure of the upper mantle, *J. Geophys. Res.*, *113*, B09303, doi:10.1029/2007JB005429.

Deen, T. J., W. L. Griffin, G. Begg, S. Y. O'Reilly, L. M. Natapov, and J. Hronsky (2006), Thermal and compositional structure of the subcontinental lithospheric mantle: Derivation from shear wave seismic tomography, *Geochem. Geophys. Geosyst.*, *7*, Q07003, doi:10.1029/2005GC001120.

Der, Z. A., and T. W. McElfresh (1976), Short-period P-wave attenuation along various paths in North America as determined from P-wave spectra of the SALMON nuclear explosion, *Bull. Seismol. Soc. Am.*, *66*, 1609–1622.

Der, Z. A., and T. W. McElfresh (1977), The relationship between anelastic attenuation and regional amplitude anomalies of short-period P waves in North America, *Bull. Seismol. Soc. Am.*, *67*, 1303–1317.

Der, Z. A., T. W. McElfresh, and A. O'Donnell (1982), An investigation of the regional variations and frequency dependence of anelastic attenuation in the mantle under the United-States in the 0.5–4 Hz band, *Geophys. J. R. Astron. Soc.*, *69*, 67–99.

Dixon, J. E., T. H. Dixon, D. R. Bell, and R. Malservisi (2004), Lateral variation in upper mantle viscosity; role of water, *Earth Planet. Sci. Lett.*, *222*, 451–467.

Durek, J. J., and G. Ekström (1996), A radial model of anelasticity consistent with long-period surface-wave attenuation, *Bull. Seismol. Soc. Am.*, *86*, 144–158.

Dziewonski, A. M., and D. L. Anderson (1981), Preliminary reference Earth model, *Phys. Earth Planet. Inter.*, *25*, 297–356.

Faul, U. H., and I. Jackson (2005), The seismological signature of temperature and grain size variations in the upper mantle, *Earth Planet. Sci. Lett.*, *234*, 119–134.

Godey, S., F. Deschamps, J. Trampert, and R. Snieder (2004), Thermal and compositional anomalies beneath the North American continent, *J. Geophys. Res.*, *109*, B01308, doi:10.1029/2002JB002263.

Goes, S., and S. van der Lee (2002), Thermal structure of the North American uppermost mantle inferred from seismic tomography, *J. Geophys. Res.*, *107*(B3), 2050, doi:10.1029/2000JB000049.

Goes, S., R. Govers, and P. Vacher (2000), Shallow mantle temperatures under Europe from P and S wave tomography, *J. Geophys. Res.*, *105*, 11,153–11,169.

Goes, S., F. J. Simons, and K. Yoshizawa (2005), Seismic constraints on temperature of the Australian uppermost mantle, *Earth Planet. Sci. Lett.*, *236*, 227–237.

Grand, S. P., and D. V. Helmberger (1984), Upper mantle shear structure of North America, *Geophys. J. R. Astron. Soc.*, *76*, 399–438.

Hammond, W. C., and E. D. Humphreys (2000), Upper mantle seismic wave attenuation: Effects of realistic partial melt distribution, *J. Geophys. Res.*, *105*, 10,987–10,999.

Houston, H., and J. E. Vidale (1994), The temporal distribution of seismic radiation during deep earthquake rupture, *Science*, *265*, 771–774.

Humphreys, E. D., and D. D. Coblentz (2007), North American dynamics and western U.S. tectonics, *Rev. Geophys.*, *45*, RG3001, doi:10.1029/2005RG000181.

Hwang, H.-J., and B. J. Mitchell (1987), Shear velocities, *Q* (sub beta), and the frequency dependence of *Q* (sub beta) in stable and tectonically active regions from surface wave observations, *Geophys. J. R. Astron. Soc.*, *90*, 575–613.

Jackson, I., J. D. Fitz Gerald, U. H. Faul, and B. H. Tan (2002), Grain-size-sensitive seismic wave attenuation in polycrystalline olivine, *J. Geophys. Res.*, *107*(B12), 2360, doi:10.1029/2001JB001225.

Kanamori, H., and D. L. Anderson (1977), Importance of physical dispersion in surface wave and free oscillation problems: Review, *Rev. Geophys.*, *15*, 105–112.

Kanamori, H., E. Hauksson, and T. Heaton (1997), Real-time seismology and earthquake hazard mitigation, *Nature (London)*, *390*, 461–464.

Karato, S. (1993), Importance of anelasticity in the interpretation of seismic tomography, *Geophys. Res. Lett.*, *20*, 1623–1626.

Karato, S., and H. A. Spetzler (1990), Defect microdynamics in minerals and solid-state mechanisms of seismic wave attenuation and velocity dispersion in the mantle, *Rev. Geophys.*, *28*, 399–421.

Lawrence, J. F., and M. E. Wysession (2006), QLM9; a new radial quality factor (*Q* (sub mu)) model for the lower mantle, *Earth Planet. Sci. Lett.*, *241*, 962–971.

Lawrence, J. F., P. M. Shearer, and G. Masters (2006), Mapping attenuation beneath North America using waveform cross-correlation and cluster analysis, *Geophys. Res. Lett.*, *33*, L07315, doi:10.1029/2006GL025813.

Lay, T., and D. V. Helmberger (1981), Body wave amplitude patterns and upper mantle attenuation variations across North America, *Geophys. J. R. Astron. Soc.*, *66*, 691–726.

Lay, T., and T. C. Wallace (1988), Multiple ScS attenuation and travel times beneath western North America, *Bull. Seismol. Soc. Am.*, *78*, 2041–2061.

Lee, C.-T. A. (2003), Compositional variation of density and seismic velocities in natural peridotites at STP conditions: Implications for seismic imaging of compositional heterogeneities in the upper mantle, *J. Geophys. Res.*, *108*(B9), 2441, doi:10.1029/2003JB002413.

Lees, J. M., and J. Park (1995), Multiple-taper spectral analysis; a stand-alone C-subroutine, *Comput. Geosci.*, *21*, 199–236.
Marone, F., and B. Romanowicz (2007), Non-linear crustal corrections in high-resolution regional waveform seismic tomography, *Geophys. J. Int.*, *170*, 460–467.
Melbourne, T., and D. V. Helmberger (1998), Fine structure of the 410-km discontinuity, *J. Geophys. Res.*, *103*, 10,091–10,102.
Mitchell, B. J. (1975), Regional Rayleigh wave attenuation in North America, *J. Geophys. Res.*, *80*, 4904–4916.
Mitchell, B. J., and L. Cong (1998), Lg coda *Q* and its relation to the structure and evolution of continents; a global perspective, *Pure Appl. Geophys.*, *153*, 655–663.
Morgan, P., and W. D. Gosnold (1989), Heat flow and thermal regimes in the continental United States, *Mem. Geol. Soc. Am.*, *172*, 493–522.
Perry, H. K. C., A. M. Forte, and D. W. S. Eaton (2003), Upper-mantle thermochemical structure below North America from seismic-geodynamic flow models, *Geophys. J. Int.*, *154*, 279–299.
Pollack, H. P., S. J. Hurter, and J. R. Johnson (1993), Heat flow from the Earth's interior: Analysis of the global data set, *Rev. Geophys.*, *31*, 267–280.
Priestley, K., and D. McKenzie (2006), The thermal structure of the lithosphere from shear wave velocities, *Earth Planet. Sci. Lett.*, *244*, 285–301.
Reid, F. J. L., J. H. Woodhouse, and H. J. van Heijst (2001), Upper mantle attenuation and velocity structure from measurements of differential S phases, *Geophys. J. Int.*, *145*, 615–630.
Romanowicz, B. (1995), A global tomographic model of shear attenuation in the upper mantle, *J. Geophys. Res.*, *100*, 12,375–12,394.
Romanowicz, B. (2008), Using seismic waves to image Earth's internal structure, *Nature*, *451*, 266–268.
Romanowicz, B., and Y. C. Gung (2002), Superplumes from the core-mantle boundary to the lithosphere: Implications for heat flux, *Science*, *296*, 513–516.
Romanowicz, B., D. E. Byrne, and S. K. Singh (1993), The Berkeley digital seismic network; upgrade status, *Seismol. Res. Lett.*, *64*, 42.
Sato, H., I. Sacks, and T. Murase (1989), The use of laboratory velocity data for estimating temperature and partial melt fraction in the low-velocity zone: Comparison with heat flow and electrical conductivity studies, *J. Geophys. Res.*, *94*, 5689–5704.
Schutt, D. L., and C. E. Lesher (2006), Effects of melt depletion on the density and seismic velocity of garnet and spinel lherzolite, *J. Geophys. Res.*, *111*, B05401, doi:10.1029/2003JB002950.
Secor, D. T., Jr., A. W. Snoke, and R. D. Dallmeyer (1986), Character of the Alleghanian Orogeny in the Southern Appalachians: Part III. Regional tectonic relations, *Geol. Soc. Am. Bull.*, *97*, 1345–1353.
Selby, N. D., and J. H. Woodhouse (2002), The *Q* structure of the upper mantle: Constraints from Rayleigh wave amplitudes, *J. Geophys. Res.*, *107*(B5), 2097, doi:10.1029/2001JB000257.
Shapiro, N. M., and M. H. Ritzwoller (2004), Inferring surface heat flux distributions guided by a global seismic model: Particular application to Antarctica, *Earth Planet. Sci. Lett.*, *223*, 213–224.
Sobolev, S. V., S. V. H. Zeyen, G. Stoll, F. Werling, R. Altherr, and K. Fuchs (1996), Upper mantle temperatures from teleseismic tomography of French Massif Central including effects of composition, mineral reactions, anharmonicity, anelasticity and partial melt, *Earth Planet. Sci. Lett.*, *139*, 147–163.
Solomon, S. C., and M. N. Toksöz (1970), Lateral variation of attenuation of P and S waves beneath the United States, *Bull. Seismol. Soc. Am.*, *60*, 819–838.
Stein, S., and M. Wysession (2003), *An Introduction to Seismology, Earthquakes, and Earth Structure*, Blackwell, Malden, Mass.
Teng, T.-L. (1968), Attenuation of body waves and the *Q* structure of the mantle, *J. Geophys. Res.*, *73*, 2195–2208.
Trampert, J., H. Paulssen, A. van Wettum, J. Ritsema, R. Clayton, R. Castro, C. Rebollar, and A. Perez-Vertti (2003), New array monitors seismic activity near the Gulf of California in Mexico, *Eos Trans. AGU*, *84*, 29.
Van der Lee, S. (2002), High-resolution estimates of lithospheric thickness from Missouri to Massachusetts, USA, *Earth Planet. Sci. Lett.*, *203*, 15–23.
Van der Lee, S., and G. Nolet (1997), Upper mantle S velocity structure of North America, *J. Geophys. Res.*, *102*, 22,815–22,838.
Warren, L. M., and P. M. Shearer (2002), Mapping lateral variations in upper mantle attenuation by stacking *P* and *PP* spectra, *J. Geophys. Res.*, *107*(B12), 2342, doi:10.1029/2001JB001195.
Yamazaki, D., and S.-i. Karato (2001), Some mineral physics constraints on the rheology and geothermal structure of Earth's lower mantle, *Am. Mineral.*, *86*, 385–391.
Yang, Y., D. W. Forsyth, and D. S. Weeraratne (2007), Seismic attenuation near the East Pacific Rise and the origin of the low-velocity zone, *Earth Planet. Sci. Lett.*, *258*, 260–268.

S. Goes, Department of Earth Science and Engineering, Imperial College London, London SW7 2AZ, UK.

Y. K. Hwang and J. Ritsema, Department of Geological Sciences, University of Michigan, 2534 C. C. Little Building, 1100 North University Avenue, Ann Arbor, MI 48109-1005, USA. (ykhwang@umich.edu)